Appl. Math. Mech. -Engl. Ed., **39**(9), 1327–1340 (2018)

Applied Mathematics and Mechanics (English Edition)

https://doi.org/10.1007/s10483-018-2365-9

Simultaneous impacts of MHD and variable wall temperature on transient mixed Casson nanofluid flow in the stagnation point of rotating sphere*

A. MAHDY†

Department of Mathematics, Faculty of Science, South Valley University, Qena 83523, Egypt

(Received Sept. 5, 2017 / Revised Mar. 22, 2018)

Abstract A numerical analysis is provided to scrutinize time-dependent magnetohydrodynamics (MHD) free and forced convection of an electrically conducting non-Newtonian Casson nanofluid flow in the forward stagnation point region of an impulsively rotating sphere with variable wall temperature. A single-phase flow of nanofluid model is reflected with a number of experimental formulae for both effective viscosity and thermal conductivity of nanofluid. Exceedingly nonlinear governing partial differential equations (PDEs) subject to their compatible boundary conditions are mutated into a system of nonlinear ordinary differential equations (ODEs). The derived nonlinear system is solved numerically with implementation of an implicit finite difference procedure merging with a technique of quasi-linearization. The controlled parameter impacts are clarified by a parametric study of the entire flow regime. It is depicted that from all the exhibited nanoparticles, Cu possesses the best convection. The surface heat transfer and surface shear stresses in the x- and z-directions are boosted with maximizing the values of nanoparticle solid volume fraction φ and rotation λ. Besides, as both the surface temperature exponent n and the Casson parameter γ upgrade, an enhancement of the Nusselt number is given.

Key words single-phase nanofluid, Casson, transient, mixed, magnetohydrodynamics (MHD), non-uniform heating

Chinese Library Classification O361
2010 Mathematics Subject Classification 76A05, 76D05, 76M20, 76D10

Nomenclature

a,	gradient of velocity at the edge (s^{-1});	g,	acceleration due to gravity ($m{\cdot}s^{-2}$);
B_0,	magnetic field (T);	Gr,	Grashof number;
C_{fx},	shear stress in x-direction;	k,	thermal conductivity ($W{\cdot}m^{-1}{\cdot}K^{-1}$);
C_{fz},	shear stress in z-direction;	M_g,	parameter of magnetic field;
c_p,	specific heat ($J{\cdot}kg^{-1}{\cdot}K^{-1}$);	Pr,	Prandtl number;
F,	non-dimensional stream function;	R,	radius of the sphere (m);

∗ Citation: MAHDY, A. Simultaneous impacts of MHD and variable wall temperature on transient mixed Casson nanofluid flow in the stagnation point of rotating sphere. *Applied Mathematics and Mechanics* (*English Edition*), **39**(9), 1327–1340 (2018) https://doi.org/10.1007/s10483-018-2365-9

† Corresponding author, E-mail: mahdy@svu.edu.eg

Re, Reynolds number;
S, velocity components in y-direction ($\mathrm{m\cdot s^{-1}}$);
Sc, Schmidt number;
t, time (s);
T, dimensional temperature (K);
(u, v, w), velocity components ($\mathrm{m\cdot s^{-1}}$);
U, ambient velocity ($\mathrm{m\cdot s^{-1}}$);
(x, y, z), Cartesian coordinates (m).

Greek symbols

β, coefficient of thermal expansion ($\mathrm{K^{-1}}$);
μ, dynamic viscosity ($\mathrm{kg\cdot m^{-1}\cdot s^{-1}}$);
λ, rotation parameter;
σ, electrical conductivity ($\mathrm{S\cdot m^{-1}}$);
ρ, fluid density ($\mathrm{kg\cdot m^{-3}}$);
θ, dimensionless temperature;
Ω, angular velocity ($\mathrm{s^{-1}}$);
ν, kinematic viscosity ($\mathrm{m^2\cdot s^{-1}}$);
γ^*, mixed convection parameter;
γ, Casson parameter;
φ, nanoparticle solid volume fraction.

Subscripts

w, conditions at the surface;
∞, conditions in the free stream;
p, solid material;
nf, nanofluid particle;
f, fluid.

1 Introduction

The Casson fluid is assorted as a non-Newtonian liquid because of its rheological characteristics in relation to the shear stress-strain. Slight values of shear strain make the Casson fluid behave as an elastic solid, whilst above a value of critical stress, it behaves as a Newtonian fluid. The Casson fluid can be depicted as a shear thinning liquid with limitless viscosity at zero shear rate, and zero viscosity at a limitless rate of shear. A number of such common examples of liquids that present Casson fluid characteristics comprise human blood, honey, tomato, sauce, and orange juice. In 1995, Casson established the Casson fluid model for viscoelastic fluid flow. Mustafa et al.[1] analyzed the analytical solution for flow and heat transfer of Casson fluid stagnation-point towards a stretching flat sheet via the homotopy analysis method (HAM). Nadeem et al.[2] presented a self-similar solution to get the solution of the governing flow equations of an electrically conducting Casson fluid flow in two lateral directions through a porous linear stretching sheet. Boyd et al.[3] analyzed the Casson fluid of steady and oscillatory blood flow. Eldabe and Salwa[4] addressed the magnetohydrodynamics (MHD) Casson fluid flow between two rotating cylinders.

Nadeem et al.[5] depicted an enhancement in the heat and mass transfer of a three-dimensional non-Newtonian Casson nanofluid and regulated the hot liquid over the lower surface of the wall by presenting a convective boundary condition. They pointed out that a Newtonian nanofluid induces downgrade skin friction at the wall with respect to the Casson nanofluid, and for a higher Prandtl number, they obtained lower thermal conductivity. Mukhopadhyay et al.[6] looked at the Casson fluid flow over an unsteady stretching surface by extending the paper of Andersson et al.[7]. Bhattacharyya[8] reported the two-dimensional MHD stagnation region flow of an electrically conducting Casson fluid and heat transfer along a stretching surface with the impact of thermal radiation. They depicted that the Casson fluid velocity boundary layer thickness becomes larger than that of Newtonian fluid due to the Casson fluid plasticity. Mahdy and Ahmed[9] looked at the unsteady mixed convection flow of a non-Newtonian Casson fluid in the stagnation point of a rotating sphere. Mahdy[10] introduced a numerical solution for heat transfer of a non-Newtonian Casson fluid outside a stretching permeable cylinder through Soret and Dufour impacts.

Speedy progress in industrial and thermal engineering operations required more efficient and more compact heat transfer systems. These systems of heat transfer liquids are applied as cooling agent. Anyway such liquids possess low thermal conductivity which badly impacts the heat transfer rate or cooling process. It was actually a defying task for scientists to improve

the liquid thermal conductivity. To do this, about a decade ago, the first endeavor was proposed by Choi and Eastman[11] and Choi et al.[12] to present the nanofluid. The base fluid with suspended nanoparticles is so-called nanofluid. Not a few liquids possess low capability of thermal conductivity. Particles of nanosized metallic (silver, titanium, and copper) are suspended in the habitual liquids in order to upgrade the property of thermal conductivity. Nanofluid applications appear for improving the capability of heat transfer of transportation, computer microchips, solid state lightening, fuel cells, biomedicine, and microelectronics. Two classes are available to incorporate nanoparticle impact on fluid flow, namely, single-phase nanofluid and two-phase nanofluid models (Sarkar[13] and Buongiorno[14]). Further, in the Tiwari and Das model, the effective fluid properties were considered. Such theoretical and experimental contributions on nanofluid heat transfer property have been carried out in Refs. [15]–[38].

Through engineering and industrial operations, heat and mass transfer is caused by buoyancy impacts due to thermal diffusion. Takhar et al.[39] used the finite difference method to get the solution for the governing boundary layer equations of unsteady free convection flow in the forward stagnation-point region of a sphere, which rotates with time-dependent angular velocity in an ambient fluid. Results illustrated that as the Prandtl number upgrades, heat transfer enhances, whilst the skin friction reduces. Chamkha et al.[40] examined the problem of unsteady MHD free convection of a rotating fluid through a rotating sphere near the equator. They detected that both the magnetic field and the surface suction reduce the shear stress, whereas they enhance the surface shear stress in the rotational direction. Anilkumar and Roy[41] introduced a new self-similar solution of unsteady mixed convection rotating fluid flow on a rotating cone with the combined impacts of both mass and thermal diffusion. Heat and mass transfer flow of an electrically conducting fluid in the stagnation point of a rotating sphere with the impact of thermal radiation was addressed by Mahdy and Ahmed[42].

The investigation of time-dependent flow of Casson nanofluid has not attracted much attention. Hence, the essential aim of the current contribution is to address unsteady MHD Casson single-phase nanofluid flow through variable wall temperature in the stagnation region of a rotating sphere. The model of traditional non-Newtonian Casson nanofluid is revised to incorporate the impacts of thermophoresis and Brownian motion. We provide quantitative and qualitative comparisons with the preceding published data to assess the accuracy of the procedure.

2 Physical model

Let us look at the problem of conjugate MHD forced and natural convection (mixed) of Casson single-phase nanofluid boundary layer flow in the forward stagnation point region of a sphere with variable wall temperature. Water represents a base fluid that contains some types of nanoparticles, e.g., alumina Al_2O_3, silver Ag, copper Cu, and titanate TiO_2. The sphere rotates with a constant angular velocity Ω around an axis parallel to the ambient free stream velocity $U(x) = ax$, as depicted in Fig. 1. Besides, the fluid has constant physical properties except for the density which creates the buoyancy force, and the viscous dissipation term is ignored.

The axis coordinates x, y, and z are measured from the forward stagnation point along the surface, perpendicular to the surface, and in the rotating direction, respectively. The Casson nanofluid is electrically conducting with existence of a magnetic field B_0 constantly applied in the z-direction. Before time $t = 0$, the sphere is assumed to be motionless in an ambient fluid, and the surface temperature is T_∞. The sphere surface temperature is instantly raised to $T_\mathrm{w} = T_\infty + dx^n$ when the time reaches $t = 0$. In addition, the rheological model equation of state for an isotropic and incompressible flow of a Casson fluid is described as[2]

$$\tau_{ij} = \begin{cases} 2(\mu_\mathrm{B} + P_y(2\pi)^{-1/2})e_{ij}, & \pi > \pi_\mathrm{c}, \\ 2(\mu_\mathrm{B} + P_y(2\pi_\mathrm{c})^{-1/2})e_{ij}, & \pi < \pi_\mathrm{c}, \end{cases}$$

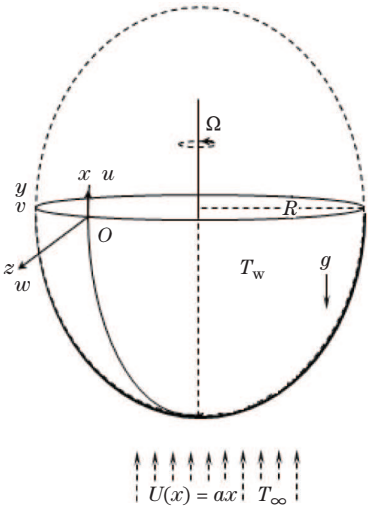

Fig. 1 Flow configuration and geometrical coordinates

in which $\pi = e_{ij}e_{ij}$ and e_{ij} represent the (i,j)th deformation rate components, π_c gives the critical value of this product based on the non-Newtonian model, μ_B means the dynamic viscosity of the non-Newtonian fluid, and P_y gives the yield stress fluid. According to the preceding presumptions and taking into account the Boussinesq approximation, the unsteady laminar boundary layer equations characterizing the mixed convection Casson single-phase nanofluid flow are[24,47]

$$\frac{\partial(xu)}{\partial x} + \frac{\partial(xw)}{\partial z} = 0, \tag{1}$$

$$\rho_{nf}\Big(\frac{\partial u}{\partial t} + u\frac{\partial u}{\partial x} + w\frac{\partial u}{\partial z} - \frac{v^2}{x}\Big) = \rho_{nf}U\frac{\mathrm{d}U}{\mathrm{d}x} + \mu_{nf}\Big(1+\frac{1}{\gamma}\Big)\frac{\partial^2 u}{\partial z^2} + g(\rho\beta)_{nf}(T-T_\infty)\frac{x}{R} + \sigma_{nf}B_0^2(U-u), \tag{2}$$

$$\rho_{nf}\Big(\frac{\partial v}{\partial t} + u\frac{\partial v}{\partial x} + w\frac{\partial v}{\partial z} + \frac{vu}{x}\Big) = \mu_{nf}\Big(1+\frac{1}{\gamma}\Big)\frac{\partial^2 v}{\partial z^2} - \sigma_{nf}B_0^2 v, \tag{3}$$

$$(\rho c_p)_{nf}\Big(\frac{\partial T}{\partial t} + u\frac{\partial T}{\partial x} + w\frac{\partial T}{\partial z}\Big) = k_{nf}\frac{\partial^2 T}{\partial z^2}. \tag{4}$$

The initial conditions are described as

$$t<0: \quad u(t,x,z) = v(t,x,z) = w(t,x,z) = 0, \quad T(t,x,z) \to T_\infty \tag{5}$$

associated with the following compatible boundary conditions:

$$t \geqslant 0: \quad u(t,x,0) = 0, \quad v(t,x,0) = \Omega x, \quad w(t,x,0) = 0, \quad T(t,x,0) = T_w = T_\infty + dx^n, \tag{6}$$

whereas the boundary conditions at ambient (i.e., $z \to \infty$) are portrayed as

$$u(t,x,\infty) \to U(x), \quad v(t,x,\infty) \to 0, \quad T(t,x,\infty) \to T_\infty. \tag{7}$$

The components of Casson nanofluid velocity in the x-, y-, and z-directions are symbolized by u, v, and w, respectively, γ refers to the Casson parameter, t is the time, R is the sphere radius, g refers to the gravity acceleration, n represents the sphere surface temperature exponent, μ_{nf}, ρ_{nf}, k_{nf}, σ_{nf}, and $(c_p)_{nf}$ refer to the nanofluid viscosity, nanofluid density, nanofluid

thermal conductivity, effective electrical conductivity, and specific heat at constant pressure, respectively, and $\beta_{\rm nf}$ indicates the expansion effective thermal volumetric coefficient. Now, the effective properties of nanofluid are described by the following formulae[43–44]:

$$\mu_{\rm nf}=\mu_{\rm f}(1-\varphi)^{-5/2},\quad \rho_{\rm nf}=(1-\varphi)\rho_{\rm f}+\varphi\rho_{\rm p},$$
$$(\rho c_p)_{\rm nf}=(1-\varphi)(\rho c_p)_{\rm f}+\varphi(\rho c_p)_{\rm p},\quad (\rho\beta)_{\rm nf}=(1-\varphi)(\rho\beta)_{\rm f}+\varphi(\rho\beta)_{\rm p},$$
$$k_{\rm nf}=k_{\rm f}\frac{k_{\rm p}+2k_{\rm f}+2\varphi(k_{\rm p}-k_{\rm f})}{k_{\rm p}+2k_{\rm f}-\varphi(k_{\rm p}-k_{\rm f})},\quad \sigma_{\rm nf}=\sigma_{\rm f}\Big(1+\frac{3(\sigma-1)\varphi}{(\sigma+2)-(\sigma-1)\varphi}\Big),\quad \sigma=\frac{\sigma_{\rm p}}{\sigma_{\rm f}},$$

where φ represents the nanoparticle solid volume fraction ($\varphi=0$ points to a regular fluid), $\rho_{\rm f}$ and $\rho_{\rm p}$ refer to the density of base fluid and nanoparticles, respectively, $(c_p)_{\rm f}$ and $(c_p)_{\rm p}$ mean the specific heat of base fluid and nanoparticles, respectively, $\sigma_{\rm f}$ and $\sigma_{\rm p}$ indicate the electrical conductivity of base fluid and nanoparticles, respectively, $\beta_{\rm f}$ and $\beta_{\rm p}$ represent the thermal volumetric coefficient of base fluid and nanoparticles, respectively, $\mu_{\rm f}$ denotes the base fluid viscosity, and $k_{\rm f}$ and $k_{\rm p}$ refer to thermal conductivity of base fluid and nanoparticles, respectively. The thermo-physical properties of the nanofluid are depicted in Table 1 as Jawad et al.[45].

Table 1 Thermo-physical properties of water and nanoparticles[45]

Physical property	Water base fluid	Cu	Ag	Al_2O_3	TiO_2
$\rho/(\mathrm{kg\cdot m^{-3}})$	997.1	8 933	10 500	3 970	4 250
$c_p/(\mathrm{J\cdot kg^{-1}\cdot K^{-1}})$	4 179	385	235	765	686.2
$k/(\mathrm{W\cdot m^{-1}\cdot K^{-1}})$	0.613	401	429	40	8.953 8
$\beta\times10^5/\mathrm{K^{-1}}$	21	1.67	1.89	0.85	0.9
$\sigma\times10^{-6}/(\mathrm{S\cdot m^{-1}})$	5.5×10^{-12}	59.6	63	36.9	2.4

Now, to convert the flow governing equations and their compatible boundary conditions into non-dimensional forms, the following non-similarity transformation are utilized:

$$\begin{cases}\eta=\Big(\dfrac{2a}{\nu_{\rm f}}\Big)^{1/2}\xi^{-1/2}\,z,\quad \xi=1-\mathrm{e}^{-at},\quad u(x,z,t)=axF'(\xi,\eta),\quad U(x)=ax,\\ v(x,z,t)=\Omega xS(\xi,\eta),\quad w=-(2a\nu_{\rm f})^{1/2}\xi^{1/2}F(\xi,\eta),\quad \theta(\eta)=\dfrac{T-T_\infty}{T_{\rm w}-T_\infty}.\end{cases}\tag{8}$$

Via the provided non-similarity transformations (8), the remaining flow governing equations (2)–(4) are mutated to a system of ordinary differential equations (ODEs) of the form

$$\frac{\mu_{\rm nf}}{\mu_{\rm f}}\Big(1+\frac{1}{\gamma}\Big)F'''+\frac{\rho_{\rm nf}}{\rho_{\rm f}}\Big(\xi FF''+\frac{1}{4}\eta(1-\xi)F''+\frac{1}{2}\xi(1-F'^2+\lambda S^2)\Big)$$
$$+\frac{1}{2}\,\frac{\sigma_{\rm nf}}{\sigma_{\rm f}}\xi M_{\rm g}(1-F')+\frac{1}{2}\,\frac{(\rho\beta)_{\rm nf}}{(\rho\beta)_{\rm f}}\xi\gamma^*\theta=\frac{1}{2}\,\frac{\rho_{\rm nf}}{\rho_{\rm f}}\xi(1-\xi)\frac{\partial F'}{\partial\xi},\tag{9}$$
$$\frac{\mu_{\rm nf}}{\mu_{\rm f}}\Big(1+\frac{1}{\gamma}\Big)S''+\frac{\rho_{\rm nf}}{\rho_{\rm f}}\xi(FS'-F'S)+\frac{1}{4}\frac{\rho_{\rm nf}}{\rho_{\rm f}}\eta\,(1-\xi)S'-\frac{1}{2}\frac{\sigma_{\rm nf}}{\sigma_{\rm f}}\xi M_{\rm g}S$$
$$=\frac{1}{2}\,\frac{\rho_{\rm nf}}{\rho_{\rm f}}\xi(1-\xi)\frac{\partial S}{\partial\xi},\tag{10}$$
$$\frac{k_{\rm nf}}{k_{\rm f}}\frac{1}{Pr}\theta''+\frac{(\rho c_p)_{\rm nf}}{(\rho c_p)_{\rm f}}\Big(\frac{1}{4}\eta(1-\xi)\theta'+\xi F\theta'-\frac{n}{2}\xi F'\theta\Big)=\frac{1}{2}\,\frac{(\rho c_p)_{\rm nf}}{(\rho c_p)_{\rm f}}\xi(1-\xi)\frac{\partial\theta}{\partial\xi}\tag{11}$$

associated with the mutated boundary layer conditions

$$\begin{cases}F(\xi,0)=F'(\xi,0)=0,\quad S(\xi,0)=1,\quad \theta(\xi,0)=1,\\ F'(\xi,\infty)\to1,\quad S(\xi,\infty)\to0,\quad \theta(\xi,\infty)\to0.\end{cases}\tag{12}$$

The resulting primes mean differentiation with respect to the non-similarity variable η, where $Pr = \frac{\mu_{\rm f}(c_p)_{\rm f}}{k_{\rm f}}$ refers to the Prandtl number, $M_{\rm g} = \frac{\sigma_{\rm f} B_0^2}{\rho_{\rm f} a}$ indicates the magnetic field parameter, $\lambda = \left(\frac{\Omega}{a}\right)^2$ indicates the rotation parameter, $\gamma^* = \frac{Gr}{Re^2}$ is the mixed convection parameter, $Re = \frac{Ux}{\nu_{\rm f}}$ is the Reynolds number, and $Gr = \frac{g\beta_{\rm f}(T_{\rm w}-T_\infty)R^3}{\nu_{\rm f}^2}$ denotes the Grashof number.

Now, the shear stresses in the x- and z-directions are described as

$$Re^{1/2}\xi^{1/2}C_{{\rm f}x} = \frac{2\mu_{\rm nf}}{\rho_{\rm f}U^2}\left(1+\frac{1}{\gamma}\right)\left(\frac{\partial u}{\partial z}\right)_{z=0} = 2\sqrt{2}\,\frac{\mu_{\rm nf}}{\mu_{\rm f}}\left(1+\frac{1}{\gamma}\right)F''(\xi,0), \tag{13}$$

$$Re^{1/2}\xi^{1/2}C_{{\rm f}z} = -\frac{2\mu_{\rm nf}}{\rho_{\rm f}U^2}\left(1+\frac{1}{\gamma}\right)\left(\frac{\partial v}{\partial z}\right)_{z=0} = -2\sqrt{2}\left(1+\frac{1}{\gamma}\right)\lambda^{1/2}S'(\xi,0). \tag{14}$$

The rate of surface heat transfer in terms of the Nusselt number takes the form

$$Re^{-1/2}\xi^{1/2}Nu = -\frac{k_{\rm nf}x}{k_{\rm f}(T_{\rm w}-T_\infty)}\left(\frac{\partial T}{\partial z}\right)_{z=0} = -\sqrt{2}\,\frac{k_{\rm nf}}{k_{\rm f}}\theta'(\xi,0). \tag{15}$$

3 Numerical scheme

Now, the highly nonlinear governing equations (9)–(11) associated with boundary conditions (12) are solved numerically via the Keller box procedure. The detail of this technique is interpreted by Cebeci and Bradshaw[46]. This method is unconditionally stable and has accuracy of second-order. Four steps are followed to obtain the numerical solutions.

Step 1 The resulting governing flow equations are mutated to a system of first-order.

Step 2 Then, the derived first-order system is approximated via formula of central difference about the mid-point.

Step 3 Now, the deduced algebraic equations are quasi-linearized via Newton's method and insert them in matrix-vector notation.

Step 4 In the end, we solve the obtained linear system via the block technique of tri-diagonal elimination.

Now, the used step size is $\eta = 0.01$ and the boundary layer thickness is $\eta_\infty = 7$. Additionally, for all the cases, the convergent criteria 10^{-6} is considered. The calculations and graphical results are produced through MATLAB software. To assess the validity and accuracy of used code, a comparison is made with previous data from the literature as a limiting case. Figure 2 is provided to assess the accuracy of the used technique. A comparison with those published by Takhar et al.[47] is made and found to be in good agreement.

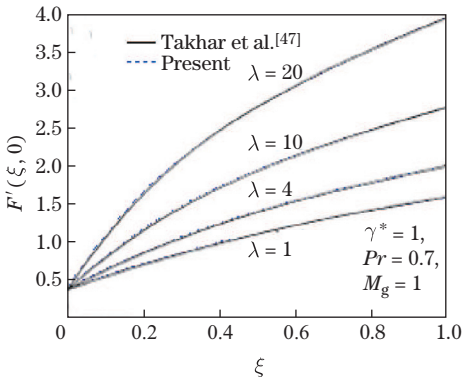

Fig. 2 Comparison data prepared by Takhar et al.[47]

4 Results and discussion

In order to address the impacts of various governing parameters of Casson nanofluid flow behavior thereabout the stagnation point of rotating sphere, numerical computations are pointed out. The ranges of such controlling parameters are the non-Newtonian Casson parameter $0.1 \leqslant \gamma \leqslant \infty$ (Newtonian fluid), the surface temperature exponent (constant wall temperature) $0 \leqslant n \leqslant 2$, the Prandtl number $0.7 \leqslant Pr \leqslant 10$, the rotation parameter $1.0 \leqslant \lambda \leqslant 50.0$, the mixed convection parameter $0.0 \leqslant \gamma^* \leqslant 5.0$, the magnetic field parameter $0.0 \leqslant M_{\mathrm{g}} \leqslant 10$, and the nanoparticle volume fraction $0.0 \leqslant \varphi \leqslant 0.1$. Now, with $n = 1$, $\lambda = 10$, $\gamma^* = 1$, $Pr = 6.2$, $\gamma = 1$, $M_{\mathrm{g}} = 3$, and $\varphi = 0.05$, Fig. 3 portrays the rate of heat transfer expressed in terms of Nusselt number Nu for some different nanoparticles, namely, Cu, Ag, Al_2O_3, and TiO_2. We notice that both Cu and Ag are close with little higher of Cu. TiO_2 gives the minimum value of Nusselt number. Similar to the shear stress $-S'(\xi, 0)$, we observe that Cu is near Ag, while Al_2O_3 is near TiO_2 (see Fig. 4).

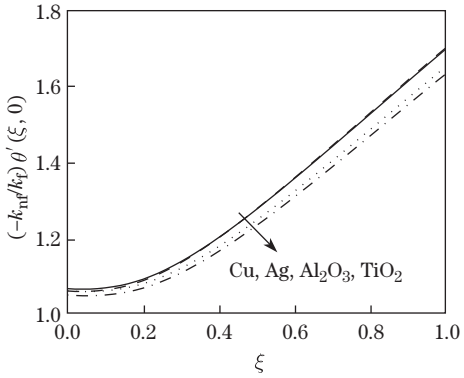

Fig. 3 Nu for some nanoparticles

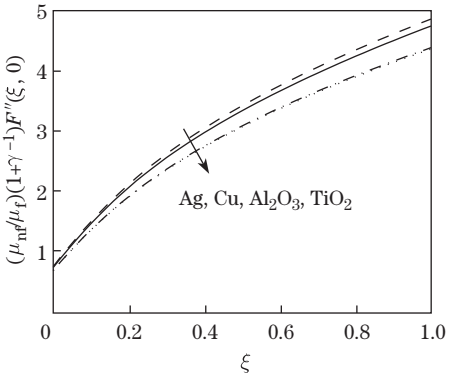

Fig. 4 $C_{\mathrm{f}z}$ for some nanoparticles

Figures 5 and 6 show the impact of power-law index of surface temperature n on the temperature curves and Nusselt number with Cu nanoparticle and for both $\varphi = 0.00$ (regular fluid) and $\varphi = 0.05$. A clear reduction in temperature curves is obtained as n upgrades (see Fig. 5). Figure 6 explains that the Nusselt number becomes larger as n upgrades. From Fig. 7, as the Casson parameter γ goes to ∞, a reduction of the non-Newtonian behavior to Newtonian behavior occurs. Therefore, the velocity boundary layer thickness for the non-Newtonian Casson fluid becomes larger than that for the Newtonian one. This is caused by the plasticity of the

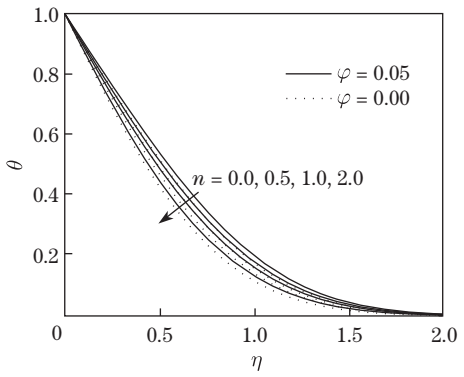

Fig. 5 θ curves for different n

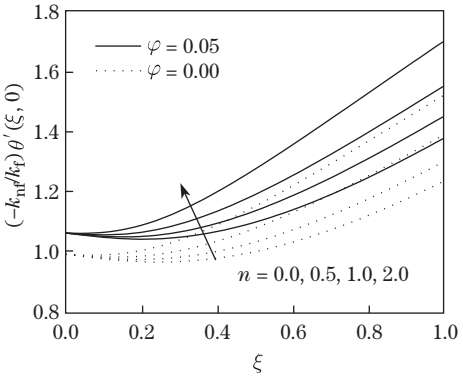

Fig. 6 Nu curves for different n

fluid that upgrades as the Casson parameter lessens which causes an upgrade in the velocity of the y-direction and the thermal boundary layer thickness. Consequently, the phenomenon of free convection is downgraded by enhancing γ. In addition, the temperature curves reduce as the Casson parameter goes from non-Newtonian fluid to Newtonian fluid, i.e., with enlarging γ (see Fig. 8).

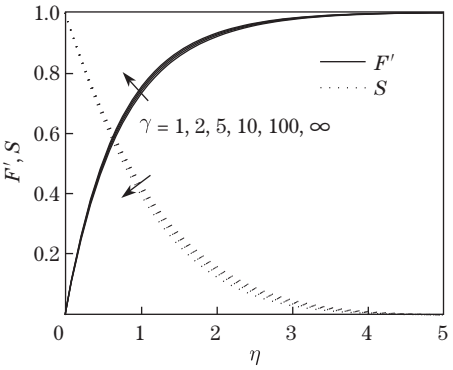

Fig. 7 F' and S curves for different γ

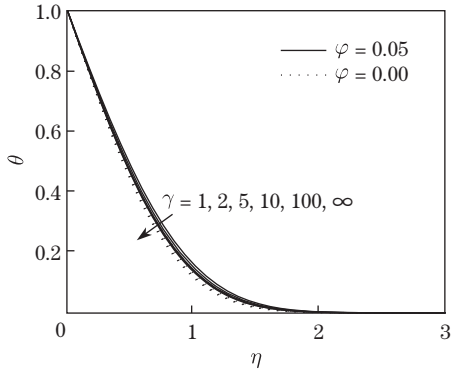

Fig. 8 Variation of θ for different γ

Besides, the variations of shear stresses in the x- and y-directions with Cu nanoparticle, i.e., $F''(\xi,0)$ and $-S'(\xi,0)$ against ξ for some values of Casson parameter γ are illustrated in Figs. 9 and 10. Both $F''(\xi,0)$ and $-S'(\xi,0)$ reduce as the Casson parameter upgrades. Per contra, the Nusselt number boosts with increasing γ as portrayed in Fig. 11. The impacts of the nanoparticle volume friction φ on the velocity profiles, the temperature distribution, the rate of heat transfer in terms of Nusselt number and shear stresses for the Cu nanofluid are presented in Figs. 12–16, respectively. As φ upgrades, $F'(\xi,\eta)$, $\theta(\xi,\eta)$, Nu, $F''(\xi,0)$, and $-S'(\xi,0)$ uplift except the velocity in the y-direction reduces. Commonly, the thermal conductivity of the nanofluid has a remarkable effect in such kinds of applications. According to this fact, one can explore the behaviors of $F'(\xi,\eta)$, $\theta(\xi,\eta)$, Nu, $F''(\xi,0)$, and $-S'(\xi,0)$ under the impact of φ. Thus, as φ upgrades, the nanofluid thermal conductivity enhances which yields a good convection. The variation of Nusselt number Nu and shear stresses in the x- and y-directions with Cu nanoparticle, i.e., $F''(\xi,0)$, $-S'(\xi,0)$, and the Nusselt number against ξ for some values of mixed convection parameter γ^* are plotted in Figs. 17–19. $-\theta'(\xi,0)$, $F''(\xi,0)$, and $-S'(\xi,0)$ increase as the mixed convection parameter γ^* upgrades which is caused by downgrade of viscous and thermal boundary layer thicknesses. This can be expounded as the positive buoyancy force acts as a pressure gradient which accelerates the fluid motion inside the boundary layer. This

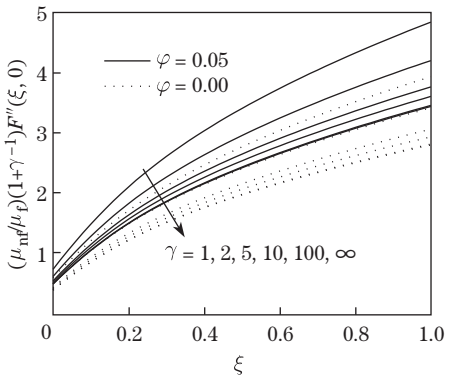

Fig. 9 C_{fx} for different γ

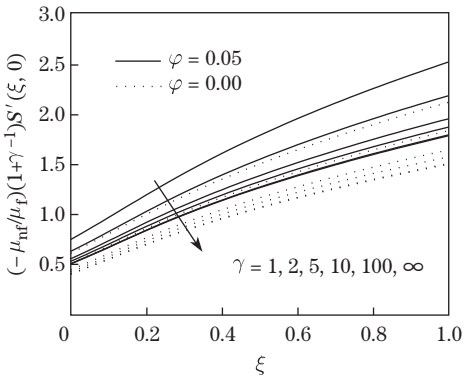

Fig. 10 C_{fz} for different γ

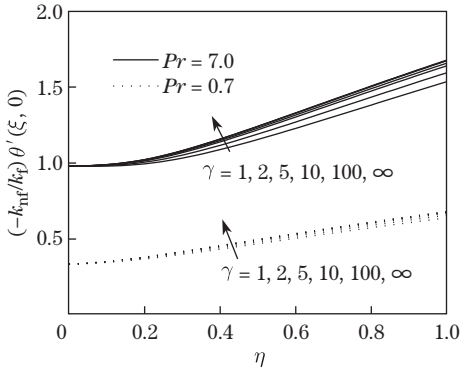

Fig. 11 Nu for different γ

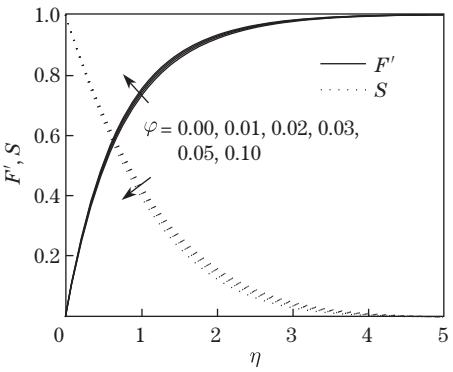

Fig. 12 F' and S curves for different φ

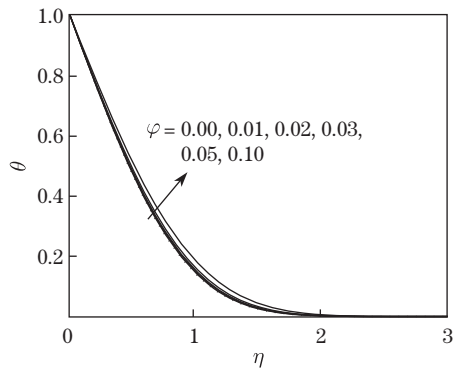

Fig. 13 θ curves for different φ

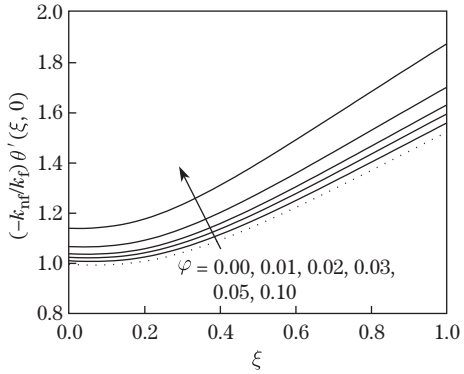

Fig. 14 Nu for different φ

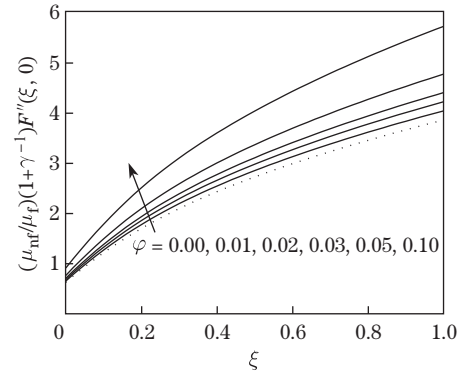

Fig. 15 $C_{\mathrm{f}x}$ for different φ

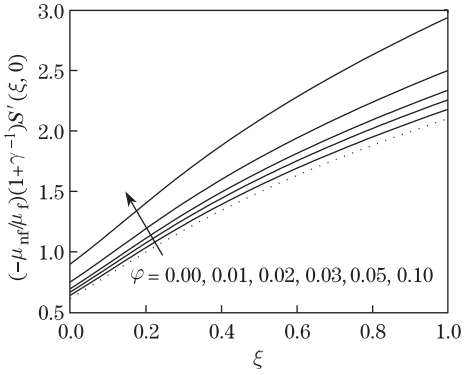

Fig. 16 $C_{\mathrm{f}z}$ for different φ

in turn minimizes the thickness of thermal and momentum boundary layers and consequently upgrades heat transfer and shear stresses at the surface.

Figures 20–22 exhibit the impact of the rotation parameter λ on the rate of heat transfer expressed in terms of Nusselt number and shear stresses, respectively, with Cu nanoparticles $\varphi = 0.05$ and Casson fluid $\gamma = 1$. An enhance in the rotation parameter λ has a strong positive impact on the shear stresses and rate of heat transfer.

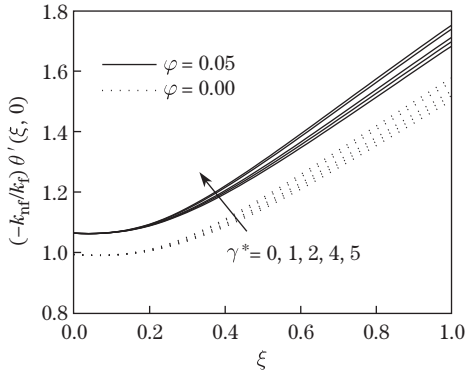

Fig. 17 Nu for different γ^*

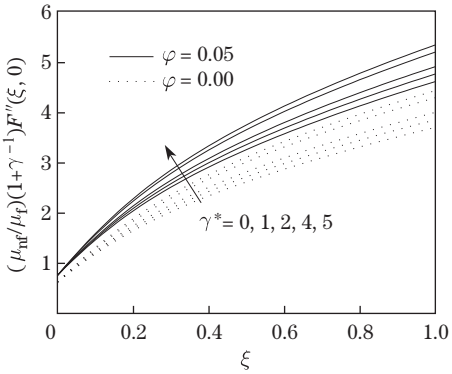

Fig. 18 C_{fx} for different γ^*

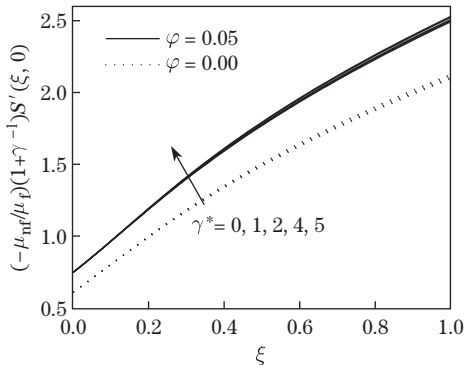

Fig. 19 C_{fz} for different γ^*

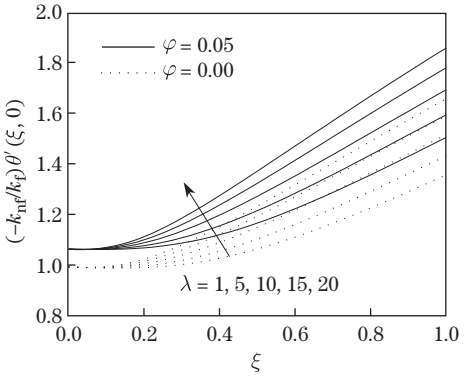

Fig. 20 Nu for different λ

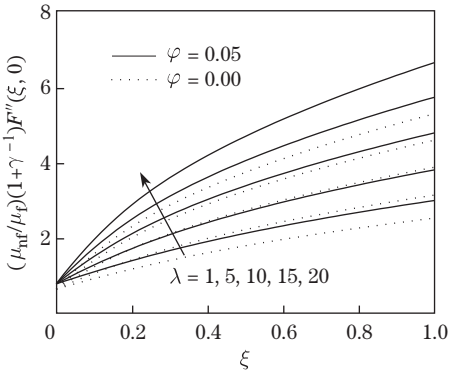

Fig. 21 C_{fx} for different λ

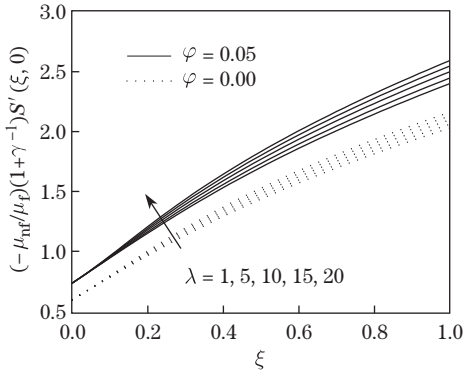

Fig. 22 C_{fz} for different λ

Nu, $F''(\xi, 0)$, and $-S'(\xi, 0)$ upgrade by increasing λ. Moreover, the velocity and thermal boundary layer thickness upgrade slightly with upgrading the rotation parameter. The reduction of momentum and thermal boundary layers leads to the increase in the velocity and temperature gradients at the wall. An increment is found in the shear stresses in both the x- and y-directions and the rate of heat transfer and temperature distribution when the magnetic field parameter M_g upgrades (see Figs. 23–26).

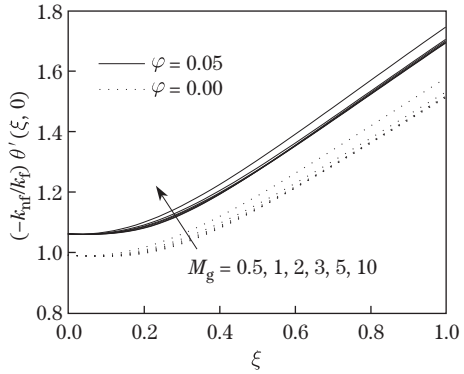

Fig. 23 Nu for different M_g

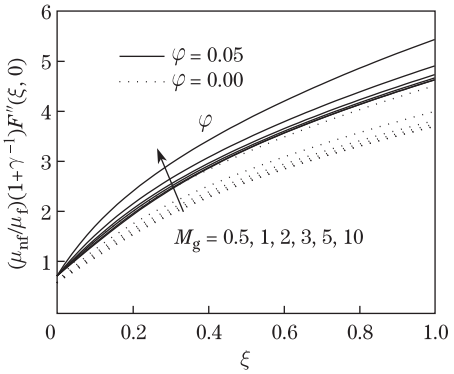

Fig. 24 C_{fx} for different M_g

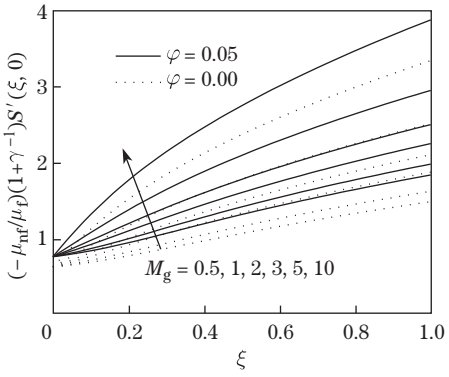

Fig. 25 C_{fz} for different M_g

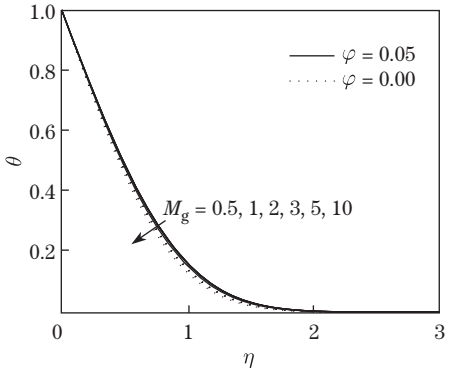

Fig. 26 θ curves for different M_g

Via the physical standpoint, when the magnetic field produces current in the conductive fluid, it creates a resistive-type force (called the Lorentz force) on the fluid in the boundary layer, which makes the motion of the fluid be slow. This downgrade of the velocity distributions improves both the velocity and thermal boundary layer thicknesses which causes an upgrade in the shear stresses in the x- and y-directions and the rate of heat transfer $\theta'(\xi, 0)$. The surface shear stresses and rate of heat transfer do not depend on the magnetic field M_g at $\xi = 0$ (at the beginning of the motion). Then, the impact of M_g upgrades with ξ. The temperature distribution reduces when M_g upgrades as portrayed in Fig. 26.

5 Remarks

The aim of our present analysis is to inspect the simultaneous impacts of variable wall temperature and MHD on the time-dependent mixed convection flow of non-Newtonian Casson nanofluid through the stagnation region according to impulsively rotating sphere. The parameters of surface shear stresses and heat transfer rate are improved by the surface temperature exponent parameter, the sphere rotation, and the buoyancy force and by using nanoparticles rather than the regular fluid. As the nanoparticle volume friction upgrades, both $F'(\xi, \eta)$ and the temperature distribution upgrade, but $S(\xi, \eta)$ downgrades. The rotation parameter λ and the Casson parameter γ tend to boost the rate of heat transfer $\theta'(\xi, 0)$. The nanoparticles can boost the heat transfer capacity of regular fluid when it is added to the base fluid. As the solid volume fraction enhances, the more impact is presented.

Acknowledgements The authors would like to express their gratitude to the reviewers for their constructive and precise suggestions.

References

[1] MUSTAFA, M., HAYAT, T., POP, I., and HENDI, A. Stagnation-point flow and heat transfer of a Casson fluid towards a stretching sheet. *Zeitschrift für Naturforschung A*, **67**, 70–76 (2012)

[2] NADEEM, S., HAQ, R. U., AKBAR, N. S., and KHAN, Z. H. MHD three-dimensional Casson fluid flow past a porous linearly stretching sheet. *Alexandria Engineering Journal*, **52**(4), 577–582 (2013)

[3] BOYD, J., BUICK, J., and GREEN, M. S. Analysis of the Casson and Carreau-Yasuda non-Newtonian blood models in steady and oscillatory flow using the lattice Boltzmann method. *Physics of Fluids*, **19**, 93–103 (2007)

[4] ELDABE, N. T. M. and SALWA, M. G. E. Heat transfer of MHD non-Newtonian Casson fluid flow between two rotating cylinders. *Journal of the Physical Society of Japan*, **64**, 41–64 (1995)

[5] NADEEM, S., HAQ, R. U., and AKBAR, N. S. MHD three-dimensional boundary layer flow of Casson nanofluid past a linearly stretching sheet with convective boundary condition. *IEEE Transactions on Nanotechnology*, **13**, 109–115 (2014)

[6] MUKHOPADHYAY, S., DE RANJAN, P., BHATTACHARRYYA, K., and LAYEK, G. C. Casson fluid flow over an unsteady stretching surface. *Ain Shams Engineering Journal*, **4**, 933–938 (2013)

[7] ANDERSSON, H. I., AARSETH, J. B., and DANDAPAT, B. S. Heat transfer in a liquid film on an unsteady stretching surface. *International Journal of Heat and Mass Transfer*, **43**, 69–74 (2000)

[8] BHATTACHARYYA, K. MHD stagnation-point flow of Casson fluid and heat transfer over a stretching sheet with thermal radiation. *Journal of Thermodynamics*, **2013**, 169674 (2013)

[9] MAHDY, A. and AHMED, S. E. Unsteady MHD convective flow of non-Newtonian Casson fluid in the stagnation region of an impulsively rotating sphere. *Journal of Aerospace Engineering*, **30**(5), 1–1 (2017)

[10] MAHDY, A. Heat transfer and flow of a Casson fluid due to a stretching cylinder with the Soret and Dufour effects. *Journal of Engineering Physics and Thermophysics*, **88**(4), 927–936 (2015)

[11] CHOI, S. U. S. and EASTMAN, J. A. Enhancing thermal conductivity of fluids with nanoparticles. *Developments Applications of Non-Newtonian Flows* (eds. SIGINER, D. A. and WANG, H. P.), FED-vol. 231/MD-ASME, New York, **66**, 99–105 (1995)

[12] CHOI, S. U. S., ZHANG, Z. G., LOCKWOOD, F. E., and GRULKE, E. A. Anomalous thermal conductivity enhancement in nanotube suspensions. *Applied Physics Letters*, **79**, 2252–2254 (2001)

[13] SARKAR, J. A critical review on convective heat transfer correlations of nanoluids. *Renewable and Sustainable Energy Reviews*, **15**, 3271–3277 (2011)

[14] BUONGIORNO, J. Convective transport in nanofluids. *Journal of Heat Transfer*, **128**, 240–250 (2006)

[15] CHOI, S. Nanofluids: from vision to reality through research. *Journal of Heat Transfer*, **131**, 1–9 (2009)

[16] MUHAMMAD, N., NADEEM, S., and HAQ, R. U. Heat transport phenomenon in the ferromagnetic fluid over a stretching sheet with thermal stratification. *Results in Physics*, **7**, 854–861 (2017)

[17] MUHAMMAD, N. and NADEEM, S. Ferrite nanoparticles Ni-$ZnFe_2O_4$, Mn-$ZnFe_2O_4$ and Fe_2O_4 in the flow of ferromagnetic nanofluid. *The European Physical Journal Plus*, **132**, 377 (2017)

[18] RASHID, M., NADEEM, S., SALEEM, S., and NOREEN, S. A. Flow and heat transfer analysis of Jeffery nano fluid impinging obliquely over a stretched plate. *Journal of the Taiwan Institute of Chemical Engineers*, **74**, 49–58 (2017)

[19] SAEED, D., REZA, H., and POP, I. Homotopy analysis method for unsteady mixed convective stagnation-point flow of a nanofluid using Tiwari-Das nanofluid model. *International Journal of Numerical Methods for Heat and Fluid Flow*, **26**(1), 40–62 (2016)

[20] ABU-NADA, E., OZTOP, H. F., and POP, I. Buoyancy induced flow in a nanofluid filled enclosure partially exposed to forced convection. *Superlattices Microstructures*, **51**(3), 381–395 (2012)

[21] MAHDY, A. and CHAMKHA, A. J. Heat transfer and fluid flow of a non-Newtonian nanofluid over an unsteady contracting cylinder employing Buongiorno's model. *International Journal of Numerical Methods and Heat Fluid Flow*, **25**(4), 703–723 (2015)

[22] NADEEM, S., RAISHAD, I., MUHAMMAD, N., and MUSTAFA, M. T. Mathematical analysis of ferromagnetic fluid embedded in a porous medium. *Results in Physics*, **7**, 2361–2368 (2017)

[23] MUHAMMED, N., NADEEM, S., and MUSTAFA, M. T. Analysis of ferrite nanoparticles in the flow of ferromagnetic nanofluid. *PloS One*, **13**(1), e0188460 (2018)

[24] NIELD, D. A. and KUZNETSOV, A. V. Thermal instability in a porous medium layer saturated by a nanofluid: Brinkman model. *Transport in Porous Media*, **81**, 409–422 (2010)

[25] MAHDY, A. and AHMED, S. E. Laminar free convection over a vertical wavy surface embedded in a porous medium saturated with a nanofluid. *Transport in Porous Media*, **91**, 423–435 (2012)

[26] AZIZ, U. R., RASHID, M., and NADEEM, S. Entropy analysis of radioactive rotating nanofluid with thermal slip. *Applied Thermal Engineering*, **112**, 832–840 (2017)

[27] SADIA, S., HINA, G., NAHEED, B., SALEEM, S., HOSSAIN, M. A., and RAMA, S. R. G. Numerical and analytical solution of nanofluid bioconvection due to gyrotactic microorganisms along a vertical wavy cone. *International Journal of Heat and Mass Transfer*, **101**, 608–613 (2016)

[28] TIWARI, R. J. and DAS, M. K. Heat transfer augmentation in a two-sided lid-driven differentially heated square cavity utilizing nanofluids. *International Journal of Heat and Mass Transfer*, **50**, 2002–2018 (2007)

[29] HADY, F. M., IBRAHIM, F. S., ABDEL-GAIED, S. M., and EID, M. R. Effect of heat generation/absorption on natural convective boundary-layer flow from a vertical cone embedded in a porous medium filled with a non-Newtonian nanofluid. *International Communications in Heat and Mass Transfer*, **30**, 1414–1420 (2011)

[30] MAHDY, A. Unsteady mixed convection boundary layer flow and heat transfer of nanofluids due to stretching sheet. *Nuclear Engineering Design*, **249**, 248–255 (2012)

[31] MAHDY, A. and HILLAL, M. E. Uncertainties in physical property effects on viscous flow and heat transfer over a nonlinearly stretching sheet with nanofluids. *International Communications in Heat and Mass Transfer*, **39**, 713–719 (2012)

[32] MUHAMMAD, N., NADEEM, S., and MUSTAFA, T. Squeezed flow of a nanofluid with Cattaneo-Christov heat and mass fluxes. *Results in Physics*, **7**, 862–869 (2017)

[33] SAEED, D., REZA, H., and POP, I. Unsteady convective heat and mass transfer of a nanofluid in Howarth's stagnation point by Buongiorno's model. *International Journal of Numerical Methods for Heat and Fluid Flow*, **25**(5), 1176–1197 (2015)

[34] SAEED, D., REZA, H., and POP, I. Axisymmetric mixed convective stagnation-point flow of a nanofluid over a vertical permeable cylinder by Tiwari-Das nanofluid model. *Powder Technology*, **311**, 147–156 (2017)

[35] CHAMKHA, A. J., GORLA, R. S. R., and GHODESWAR, K. Nonsimilar solution for natural convective boundary layer flow over a sphere embedded in a porous medium saturated with a nanofluid. *Transport in Porous Media*, **86**(1), 13–22 (2010)

[36] SAEED, D. and POP, I. Free-convective flow of copper/water nanofluid about a rotating down-pointing cone using Tiwari-Das nanofluid scheme. *Advanced Powder Technology*, **28**, 900–909 (2017)

[37] NADEEM, S., KHAN, A. U., and SALEEM, S. A comparative analysis on different nanofluid models for the oscillatory stagnation point flow. *The European Physical Journal Plus*, **131**, 261 (2016)

[38] MAKINDE, O. D. and AZIZ, A. Boundary layer flow of a nanofluid past a stretching sheet with a convective boundary condition. *International Journal of Thermal Sciences*, **50**, 1326–1332 (2011)

[39] TAKHAR, H. S., SLAOUTI, A., KUMARI, M., and NATH, G. Unsteady free convection flow in the stagnation-point region of a rotating sphere. *International Journal Non-Linear Mechanics*, **33**(5), 857–865 (1998)

[40] CHAMKHA, A. J., TAKHAR, H. S., and NATH, G. Unsteady MHD rotating flow over a rotating sphere near the equator. *Acta Mechanica*, **164**(1/2), 31–46 (2003)

[41] ANILKUMAR, D. and ROY, S. Self-similar solution of the unsteady mixed convection flow in the stagnation point region of a rotating sphere. *Heat and Mass Transfer*, **40**(6/7), 487–493 (2004)

[42] MAHDY, A. and AHMED, S. E. Unsteady MHD double diffusive convection in the stagnation region of an impulsively rotating sphere in the presence of thermal radiation effect. *Journal of the Taiwan Institute of Chemical Engineers*, **58**, 173–180 (2016)

[43] OZTOP, H. F. and ABU-NADA, E. Numerical study of natural convection in partially heated rectangular enclosures filled with nanofluids. *International Journal of Heat and Fluid Flow*, **29**, 1326–1336 (2008)

[44] DAS, S. and JANA, R. N. Natural convective magneto-nanofluid flow and radiative heat transfer past a moving vertical plate. *Alexandria Engineering Journal*, **54**, 55–64 (2015)

[45] JAWAD, R., AZIZAH, M. R., and ZURNI, O. Numerical investigation of copper-water (Cu-water) nanofluid with different shapes of nanoparticles in a channel with stretching wall: slip effects. *Mathematical and Computational Applications*, **21**, 43–58 (2016)

[46] CEBECI, T. and BRADSHAW, P. *Physical and Computational Aspects of Convective Heat Transfer*, Springer, Berlin (1984)

[47] TAKHAR, H. S., CHAMKHA, A. J., and NATH, G. Unsteady laminar MHD flow and heat transfer in the stagnation region of an impulsively spinning and translating sphere in the presence of buoyancy forces. *Heat and Mass Transfer*, **37**, 397–402 (2001)